Wireless Personal Communications (2022) 122:3719–3740
https://doi.org/10.1007/s11277-021-09108-5

Two Energy Harvesting Protocols for SWIPT at UAVs in Cooperative Relaying Networks of IoT Systems

Huu Q. Tran[1]

Accepted: 5 September 2021 / Published online: 11 October 2021

Abstract
This paper presents two protocols in non-orthogonal multiple access (NOMA) network, namely base station (BS), based power splitting protocol (PSR) and BS based time switching protocol (TSR), for simultaneously wireless information and power transmission (SWIPT) based unmanned aerial vehicles (UAVs) which are employed in power domain NOMA based UAV communication network. The system model with k types of the UAV, one BS, and two users' devices is investigated in our work. Besides, a strategy of UAV selection is also studied. Closed-form expressions of outage probability and throughput for UAVs and both users' devices are derived. In particular, the outage probability is determined for both perfect and imperfect SIC. The numerical results show that the performance for BS-based PSR outperforms that for BS-based TSR. The analytical results match Monte Carlo simulations.

Keywords Non-orthogonal multiple access · NOMA · IoT · PSR · TSR · UAV · SWIPT · Energy harvesting · Relaying

1 Introduction

Unmanned aerial vehicles (UAVs) [1, 2] are flying devices without a human pilot onboard and is a type of the unmanned vehicle developed for rescues and military applications [3]. In areas where communication infrastructure is destroyed or the radio frequency (RF) signal transmission can not reach the desired destination, thus existing methods are limited by space and environment. To overcome these challenges, the UAVs are employed as BSs/APs/relays to aid the wireless communications of ground nodes due to their mobility, 3D coverage, and agility [4].

Currently, NOMA is recognized as a potential candidate and considered by many researchers for the fifth generation (5G) network and beyond in the last decade [5–8]. Compared to conventional OMA, NOMA shows advantages such as low latency, high spectral efficiency, high energy efficiency, and user fairness [9–11]. The critical concept of NOMA is to serve multiple users on the same frequency resource. In NOMA, with the assistance

✉ Huu Q. Tran
tranquyhuu@iuh.edu.vn

[1] Industrial University of Ho Chi Minh City (IUH), Ho Chi Minh City, Vietnam

of superposition coding (SC) and successive interference cancellation (SIC) mechanism [12], the signals of users are combined at the transmitter and decoded at the receiver, sequentially.

NOMA-based UAV communication was studied by several researchers [13, 14]. In [14], a UAV-enabled downlink NOMA system was investigated. This system consisted of two ground users, and one flying base station acted UAV. The outage probability for both ground users was derived. The outage performance for NOMA was better than that for OMA. In [15], a wireless system with distributed ground terminals and a flying base station acted UAV was studied. The throughput gains for the case of a mobile UAV base station were superior to the case of a static UAV base station in delay-tolerant applications. In [16], a UAV aided NOMA network consisted of BS, UAV, and ground users in which the BS and UAV cooperated with each other to communicate with these ground users. The sum-rate was optimized between the NOMA precoding and trajectory.

Although the UAVs have demonstrated their benefits in rescue, civil and military applications, they are still limited by a power supply. Solving energy harvesting issues in the UAVs paves the way for the development of UAV based 5G networks. In [17], an account of the applicability of NOMA for UAV-aided communication systems was studied. The relationship between altitude and energy efficiency of a UAV was considered. Two cases inspired the solution to the optimization problem, namely altitude fixed NOMA and altitude optimized NOMA, which were exploited to boost the spectral efficiency and energy efficiency. In [18], the authors proposed a UAV enabled wireless power transfer architecture to enhance the energy transfer efficiency. In [19], the throughput maximization problem of UAV-based cooperative communication systems for both decode-and-forward (DF) and amplify-and-forward (AF) protocols were investigated. In these systems, the UAV acted as a mobile relay. The transmission capacity of the UAV depended on the energy harvesting from the source.

In this paper, we proposed a system model along with two simultaneous energy harvesting and information processing protocols based on PSR and TSR for UAV-assisted cooperative relaying SWIPT NOMA. The best UAV selection is solved by repeat algorithms. Closed-form expressions of the performance metric are derived.

The main contribution of our work in this paper is summarized as follows:

- We propose a system model along with two energy harvesting protocols based on PSR and TSR, namely BS-based PSR and BS-based TSR, for a cooperative relaying SWIPT NOMA system. This model consists of one BS and k types of UAVs and two users' devices. In addition, we also compare the performance in terms of outage probability and throughput between two these protocols.
- We propose an algorithm to achieve the best UAV for information processing.
- Closed-form expressions of outage probability and throughput are derived for our system model in cases of perfect and imperfect SIC.
- The simulation results show that the outage performance, as well as the throughput for BS-based PSR are enhanced over that for BS-based TSR.

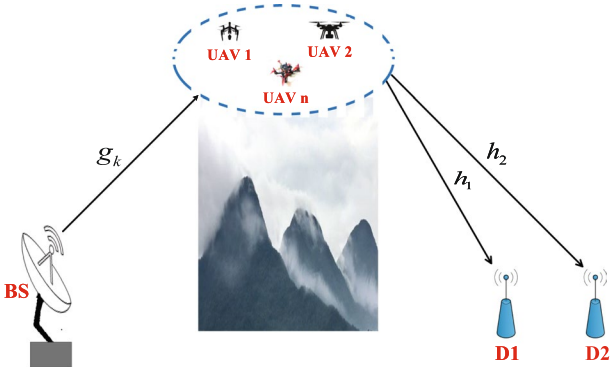

Fig. 1 A general system model

2 System Model

The system model under investigation consists of k types of UAVs, where $k = 1, 2, ..., K$, and two users' devices, i.e., D_1 and D_2, as shown in Fig. 1. One BS acts as a source unit in the system. Let d_k denote the distance between UAV_k and BS. It is assumed that all UAV_k are connected to BS via wireless connections with perfect synchronous signals.

In a wireless environment, downlink channel from the BS to UAV_k is assumed to be the flat fading channel g_k and n_k is the additive white Gaussian noise (AWGN) at UAV_k with zero mean and variance of σ_k^2.

Their expectations are $E\left[\left|g_k\right|^2\right] = d_k^{v_k}$ and $E\left[\left|n_k\right|^2\right] = \sigma_k^2$, where v_k is the path-loss of the channel model.

Assuming that UAVs operate within the coverage of the BS. The transmitted signal from the BS to UAV_k is x_k, and its expectation is $E\left[\left|x_k\right|^2\right] = 1$.

The BS transmits the signal to users using multiple UAVs. The UAV_k is equipped with a single antenna and operates in half-duplex (HD) communication mode.

In our work, we consider the case of the best UAV selection among UAVs. Moreover, all UAVs are provided via wireless energy from the BS along with conventional batteries. The channel from the BS to UAV_k and from UAV_k to users is the flat Rayleigh block fading.

As shown in Fig. 1, $g_k \sim CN\left(0, \Omega_k\right)$ is the channel coefficient of the BS and UAV_k. $\text{n}_k, \text{n}_{Di} \sim CN(0, 1)$ are the AWGNs at UAV_k and D_i, respectively. $h_i \sim CN\left(0, \Omega_{Di}\right)$ is the channel coefficient of the UAV_k and D_i, with $i \in \{1, 2\}$. Because the shadowing impact and path-loss of h_2 are less than that of h_1, the relation between Ω_{D1} and Ω_{D2} satifies $\Omega_{D1} < \Omega_{D2}$.

2.1 Energy Harvesting at UAV_k

At UAV_k, we consider two energy harvesting mechanisms including BS-based PSR and BS-based TSR at D_1

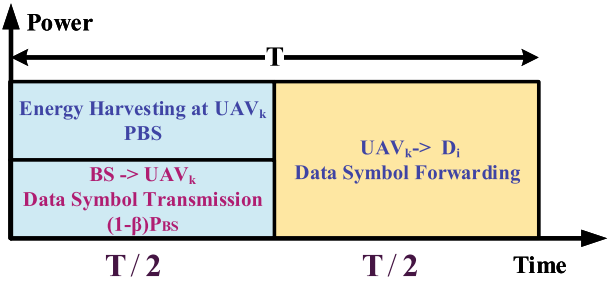

Fig. 2 BS-based PSR protocol of Energy harvesting system

2.1.1 BS-Based PSR Protocol of Energy Harvesting at UAV_k

Figure 2 describes the communication block diagram using BS-based PSR protocol for harvesting energy at UAV_k in the time block of T. It is assumed that the BS transmits the information to UAV_k in the half-block of T while the information is transmitted from UAV_k to users in the remaining time of T.

The decoded signal at the BS is given by

$$X_{BS} = (\sqrt{\Theta_1 P_{BS}} x_1 + \sqrt{\Theta_2 P_{BS}} x_2) \tag{1}$$

Applying the signal superposition coding at the BS, the observed signal at UAV_k is given by

$$y_{UAV} = \sqrt{P_{\mathrm{BS}}} g_k \left(\sqrt{\Theta_1} x_1 + \sqrt{\Theta_2} x_2 \right) + \mathrm{n}_k \,, \tag{2}$$

where P_{BS} denotes the transmit power at the BS.

By employing BS-based PSR protocol, UAV_k divides the received energy into: i) harvested energy, and ii) energy for processing the information. Let $0 < \beta < 1$ denote the power ratio. The harvested energy at UAV_k can be given by

$$E_H^{PSR} = \sum_{k=1}^{K} \beta_{k,} \eta_{k,} \rho_k |g_k|^2 (T/2) \,, \tag{3}$$

where $\rho_k \overset{\Delta}{=} P_k / \mathrm{w}_k$ represents the transmit signal-to-noise ratio (SNR) and β_k is the power splitting ratio at the UAV_k, $0 < \beta_k < 1$.

Then, the power of UAV_k for BS-based PSR protocol can be determined from (3) as follows

$$P_{UAV}^{PSR} = \frac{E_H^{PSR}}{(T/2)} = \frac{\beta_k \eta_k \rho_k |g_k|^2 (T/2)}{(T/2)} = \beta_k \eta_k \rho_k |g_k|^2 \,, \tag{4}$$

It is assumed that β_k values at UAV_k, as well as η_k at UAVs, are equal. Where η_k is the energy conversion efficiency at the UAV_k and $0 < \eta_k \leq 1$. For simplicity, $0 < \eta \leq 1$ is named the energy harvesting efficiency. η depends on the energy conversion process from RF signal to direct current in the receiver at UAV_k.

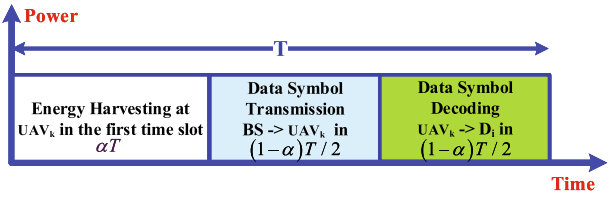

Fig. 3 BS-based TSR protocol of Energy harvesting system

2.1.2 BS-Based TSR Protocol of Energy Harvesting at UAV_k

Figure 3 illustrates the BS-based TSR protocol of the energy harvesting (EH) system. In this figure, T is the time block where the information is transmitted from BS to UAV_k, and $0<\alpha<1$ is the time block fraction where UAV_k harvests the energy from BS. The first time block of T, i.e., αT, is utilized for EH while the remaining time block, i.e., $(1-\alpha)T$, is utilized for forwarding the information. In the $(1-\alpha)T$, the half of this, i.e., $(1-\alpha)T/2$, is dedicated to transmitting data from BS to UAV_k and the remaining $(1-\alpha)T/2$ is for forwarding data from UAV_k to user k. The harvested energy at UAV_k is given by

$$\mathrm{E}_H^{TSR} = \sum_{k=1}^{K} \alpha\eta_{k,}\rho_{k,}\left|\mathrm{g_k}\right|^2 T \tag{5}$$

Therefore, the power of UAV_k for BS-based TSR protocol can be determined from (5) as follows

$$P_{UAV}^{TSR} = \frac{E_H^{\mathrm{TSR}}}{(1-\alpha)(T/2)} = \frac{2\alpha\eta_k\rho_k\left|g_k\right|^2}{1-\alpha} \tag{6}$$

It is noted that both BS-based PSR and BS-based TSR protocols are considered in this work, where the UAV_k selection is based on instantaneously technical specifications of the channel relating to the first hopping step. The BS continuously observes the quality of the connection between its own and UAV_k under the local feedback signals. From these signals, the best link between the BS and UAV_k is selected for data transmission. By grouping UAV_k multi-relays, the UAV with the best conditions is selected. This strategy is expressed by

$$k^* = \arg \underbrace{\max}_{k=1,2,\ldots,K} \left|g_k\right|^2 \tag{7}$$

We assume that the harvested energy is consumed by UAV_k to forward the signal to D_1 and D_2. The power for the transmitting-receiving circuit of UAV_k is negligible over the power for transmitting signal.

We can briefly describe the operation of the system as follows. Each communication block occupies two-time slots. All blocks are normalized to the unit. In the first time slot, the BS transmits the superimposed signal, i.e., $\sqrt{\Theta_1}x_1 + \sqrt{\Theta_2}x_2$, where x_i and Θ_i denote the signal and power allocation coefficients of D_i, respectively. The expression of $(\Theta_1 + \Theta_2)$ satisfies 1. Without loss of generality, we assume $\Theta_2 \geq \Theta_1$.

In downlink power domain NOMA, SIC and superimposed coding are two key mechanisms utilized to decode the received signals at receivers and to code the transmitted signals at transmitters, respectively. Thus, the SIC process is only considered at UAVs to achieve the best data forwarding, as well as D_1 and D_2, are allocated a higher power in our work. For instance, at UAV_k, the best UAV first decodes symbol x_2 by treating symbol x_1 as noise and then performs the SIC process to achieve signal x_1. Therefore, the signal to interference plus noise ratio (SINR) for symbol x_2 and signal to noise ratio (SNR) for symbol x_1 are respectively given by

$$\gamma_{2,UAV_k} = \frac{\Theta_2 P_{BS}|g_k|^2}{\Theta_1 P_{BS}|g_k|^2 + 1} \tag{8}$$

$$\gamma_{1,UAV_k} = \Theta_1 P_{BS}|g_k|^2 \tag{9}$$

It is noted from Fig. 1 that UAV_k processes signals x_1 and x_2 during the first time slot, then the selected UAV sends the signal $\sqrt{P^X_{UAV}}\left(\sqrt{\Theta_1}x_1 + \sqrt{\Theta_2}x_2\right)$ to two users D_1 and D_2 during the second time slot, where $X \in (PSR, TSR)$.

Thus, the received signal at D_1 combined by x_1, x_2 and noise is given by

$$y_{Di} = \sqrt{P^X_{UAV}}h_i\left(\sqrt{\Theta_1}x_1 + \sqrt{\Theta_2}x_2\right) + \mathrm{n}_{Di}\,, \tag{10}$$

where h_i is the channel gain between the selected UAV and D_i.

From (10), the SINR at D_2 is determined by applying SIC, i.e., D_2 decodes x_2 while treating x_1 as noise, as follows:

$$\gamma_{2,D_2} = \frac{\Theta_2 P^X_{UAV}|h_2|^2}{\Theta_1 P^X_{UAV}|h_2|^2 + 1} \tag{11}$$

Similarly, since both x_1 and x_2 are in D_1, it is necessary for SIC to decode its own symbol x_1. To perform SIC, D_1 decodes symbol x_2 by treating symbol x_1 as a noise according to their priority power level and cancels x_1 using SIC to obtain symbol x_1. Therefore, the SINR for x_2 at D_1 is given by

$$\gamma_{2,D_1} = \frac{\Theta_2 P^X_{UAV}|h_1|^2}{\Theta_1 P^X_{UAV}|h_1|^2 + 1} \tag{12}$$

The SNR for x_1 at D_1 decoded by its own D_1 is given by

$$\gamma_{1,D_1} = \Theta_1 P^X_{UAV}|h_1|^2 \tag{13}$$

3 Performance Analysis

3.1 Outage Behaviour at UAVs

3.1.1 The Exact Outage Behaviour of x_1 at UAV_k

The outage probability $P_{x_1}^{UAV_k}$ at UAV is the probability where UAV cannot decode completely since the SINR/SNR of x_2 is below the threshold γ_{th2} and the SINR of x_1 is below the threshold γ_{th1}, with $\gamma_{th1} = 2^{\frac{2R_1}{1-\alpha}} - 1$, where R_1 is the target data rate of D_1. From (8) and (9), the expression of $P_{x_1}^{UAV_k}$ is given by

$$\begin{aligned} P_{x_1}^{UAV_k} &= \Pr\left\{\gamma_{2,UAV_k} < \gamma_{th2}, \gamma_{1,UAV_k} < \gamma_{th1}\right\} \\ &= 1 - \sum_{k=1}^{K} (-1)^{k-1} \binom{K}{k} \exp\left(-\frac{k\varsigma}{\Omega_2}\right) \end{aligned} \tag{14}$$

Proof see "Appendix 1".

3.1.2 The Exact Outage Behaviour of x_2 at UAV_k

Similar to Sect. 3.1.1, the outage probability $P_{x_2}^{UAV_k}$ at UAV is defined as the probability at which the UAV can not successfully decode x_2 due to the SINR/SNR values below the threshold γ_{th2}. From (8), we can express the $P_{x_2}^{UAV_k}$ by

$$\begin{aligned} P_{x_2}^{UAV_k} &= \Pr\left\{\gamma_{2,UAV_k} < \gamma_{th2}\right\} \\ &= 1 - \Pr\left\{\frac{\psi_I \Theta_2 P_{BS} |g_k|^2}{\psi_I \Theta_1 P_{BS} |g_k|^2 + 1} > \gamma_{th2}\right\}, \end{aligned} \tag{15}$$

where $\psi_I = 1 - \beta$ and $\psi_I = \frac{1-\alpha}{2}$ are the information processing coefficients for BS-based PSR and BS-based TSR protocols, respectively. $\gamma_{th2} = 2^{\frac{2R_2}{1-\alpha}} - 1$ and R_2 is the target data rate of D_2. Given $|g_k|^2 = A$, $|h_1|^2 = B$ and $|h_2|^2 = C$ are the channel gains of the BS-the best UAV and the best UAV-D_1 and D_2 links, respectively. It is assumed that all channel gains are modelized independently. Random variables are Rayleigh distribution. Thus, $|g_k|^2$, $|h_1|^2$ and $|h_2|^2$ have exponential distributions as follows

$$f_X(x) = \sum\nolimits_{k=1}^{K} (-1)^{k-1} \binom{K}{k} \frac{k}{\Omega_1} \exp\left(-\frac{kx}{\Omega_1}\right) \tag{16}$$

$$f_B(b) = \frac{1}{\Omega_2} \exp\left(-\frac{y}{\Omega_2}\right), F_B(b) = 1 - \exp\left(-\frac{b}{\Omega_2}\right), \tag{17}$$

where f and F are cumulative density function and probability density function, respectively. $\Omega_1 = E\left\{|g_k|^2\right\}$, $\Omega_2 = E\left\{|h_1|^2\right\}$ and $\Omega_3 = E\left\{|h_2|^2\right\}$ are coefficients of the random variables.

Then, the expression of $P_{x_2}^{UAV_k}$ can be rewritten by

$$
\begin{aligned}
P_{x_2}^{UAV_k} &= 1-\Pr\left\{\psi_I\Theta_2 P_{BS}A > \psi_I\gamma_{th2}\Theta_1 P_{BS}A+\gamma_{th2}\right\}\\
&= 1-\Pr\left\{A\left(\psi_I\Theta_2 P_{BS}-\psi_I\gamma_{th2}\Theta_1 P_{BS}\right) > \gamma_{th2}\right\}\\
&= 1-\Pr\left\{A > \frac{\gamma_{th2}}{\psi_I P_{BS}\left(\Theta_2-\gamma_{th2}\Theta_2\right)}\right\}\\
&= 1-F_A\left(\frac{\gamma_{th2}}{\psi_I P_{BS}\left(\Theta_2-\gamma_{th2}\Theta_1\right)}\right)\\
&= 1-\sum_{k=1}^{K}(-1)^{k-1}\binom{K}{k}\exp\left(-\frac{k\gamma_{th2}}{\Omega_2\psi_I P_{BS}\left(\Theta_2-\gamma_{th2}\Theta_1\right)}\right)
\end{aligned}
\tag{18}
$$

3.2 The Exact Outage Behaviour at the User

3.2.1 The Exact Outage Behaviour of x_1 at D_1

The SIC process can occur incompletely SIC. Thus, in this section, two cases of perfect and imperfect SIC are considered at both k^* and D_1

(a) For perfect SIC From Fig. 1, it is seen that the SIC is performed at D_1 to remove signal x_2 before detecting its own signal. In the case of perfect SIC at D_1, the $P_{x_1}^{OP}$ is defined as the best UAV or D_1 can not successfully decode signal x_1 due to the SNR below the threshold value. Then, $P_{x_1}^{OP}$ is given by

$$
\begin{aligned}
P_{x_1}^{OP} &= \Pr\left(\min\left(\gamma_{1,UAV_k},\gamma_{1,D_1}\right)\le\gamma_{th1}\right)\\
&= 1-\Pr\left(\Theta_1 P_{BS}\left|g_k\right|^2 > \gamma_{th1}, \Theta_1 P_{UAV}^{X}\left|h_1\right|^2 > \gamma_{th1}\right)
\end{aligned}
\tag{19}
$$

First, let us consider the outage probability for BS-based PSR protocol as follows: By substituting P_{UAV}^{PSR} from (4) into (19), the outage probability of the signal x_1 is given by

$$
\begin{aligned}
P_{x_1}^{OP} &= 1-\Pr\left(\left|g_k\right|^2 > \frac{\gamma_{th1}}{\Theta_1 P_{BS}}, \left|h_1\right|^2 > \frac{\gamma_{th1}}{\Theta_1\beta\eta P_{BS}\left|g_k\right|^2}\right)\\
&= 1-\Pr\left(A > \frac{\gamma_{th1}}{\Theta_1 P_{BS}}, C > \frac{\gamma_{th1}}{A\Theta_1\beta\eta P_{BS}}\right)
\end{aligned}
\tag{20}
$$

This outage probability can be expressed as follows

$$
P_{x_1}^{OP} = 1-\int_u^{\infty}\left[1-F_C\left(\frac{v}{a}\right)\right]f_A(a)da\,,
\tag{21}
$$

where $u=\frac{\gamma_{th1}}{\Theta_1 P_{BS}}$ and $v=\frac{\gamma_{th1}}{\Theta_1\beta\eta P_{BS}}$ are for the BS-based PSR protocol, $v=\frac{\gamma_{th1}(1-\alpha)}{2\Theta_1\alpha\eta P_{BS}}$ is for the BS-based TSR protocol. Applying Taylor series expansion as well as substituting CDF and PDF functions of A and C into (21), we can obtain the expanded $P_{x_1}^{OP}$ expression as follows (see Eq. (22) at the top of the next page)

$$P_{x_1}^{OP} = 1 - \sum_{k=1}^{K} (-1)^{k-1} \binom{K}{k} \frac{k}{\Omega_2} \int_u^{\infty} \exp\left(-\frac{v}{\Omega_3 x}\right) \exp\left(-\frac{ka}{\Omega_2}\right) da$$
$$= 1 - \sum_{k=1}^{K} (-1)^{k-1} \binom{K}{k} \frac{k}{\Omega_2} \sum_{n=1}^{K_t} \frac{(-1)^n}{n!} \left(\frac{v}{\Omega_3}\right)^n \left(\frac{1}{u}\right)^{n-1} E_n\left(\frac{ku}{\Omega_2}\right) \tag{22}$$

b) For imperfect SIC In this case, signal x_2 does not appear at D_1 and becomes interference. The SINR of symbol x_1 at k^* and D_1 is correspondingly given by

$$\gamma_{1,UAV_k} = \frac{\Theta_1 P_{BS} |g_k|^2}{\Theta_2 \rho_2 P_{BS} |g_k|^2 + 1} \tag{23}$$

$$\gamma_{1,D1} = \frac{\Theta_1 P_{UAV}^X |h_1|^2}{\Theta_2 \rho_1 P_{UAV}^X |h_1|^2 + 1}, \tag{24}$$

where $0 < \rho_j \leq 1$, $j \in \{1, 2, ..., N_k\}$, represents the remaining noise level due to imperfect SIC at k^* and D_1. In particular, $\rho_j = 1$ and $\rho_j = 0$ relate to the cases without SIC and perfect SIC, respectively. From (23) and (24), the outage probability of x_1 for imperfect SIC is given by (see Eq. (25) at the top of the next page)

$$P_{x_1,D_1}^{I\_SIC} = \Pr\left[\min\left(\gamma_{1,UAV_k}, \gamma_{1,D1}\right) \leq \gamma_{th1}\right] = 1 - \Pr\left[A \geq \frac{\gamma_{th1}}{P_{BS}(\Theta_1 - \gamma_{th1}\Theta_2\rho_2)}, C \geq \frac{\gamma_{th1}}{A\psi_E P_{BS}(\Theta_1 - \gamma_{th1}\Theta_2\rho_1)}\right] \tag{25}$$

Proof see "Appendix 2" Solving (25), we can obtain

$$P_{x_1,D_1}^{I\_SIC} = 1 - \int_w^{\infty} \left[1 - F_C\left(\frac{s}{a}\right)\right] f_A(a) da, \tag{26}$$

where $w = \frac{\gamma_{th1}}{P_{BS}(\Theta_1 - \gamma_{th1}\Theta_2\rho_2)}$, $s = \frac{\gamma_{th1}}{\psi_E P_{BS}(\Theta_1 - \gamma_{th1}\Theta_2\rho_1)}$ Then, by some calculation processes, the $P_{x_1,D_1}^{I\_SIC}$ can be rewritten by (see Eq. (27) in the next page)

$$P_{x_1,D_1}^{I\_SIC} = 1 - \sum_{k=1}^{K} (-1)^{k-1} \binom{K}{k} \frac{k}{\Omega_2} \int_w^{\infty} \exp\left(-\frac{s}{\Omega_3 a}\right) \exp\left(-\frac{ka}{\Omega_2}\right) da$$
$$= 1 - \sum_{k=1}^{K} (-1)^{k-1} \binom{K}{k} \frac{k}{\Omega_2} \sum_{n=0}^{K_t} \frac{(-1)^n}{n!} \left(\frac{d}{\Omega_3}\right)^n \left(\frac{1}{w}\right)^{k-1} E_n\left(\frac{kw}{\Omega_2}\right) \tag{27}$$

3.2.2 The Exact Outage Behaviour of x_2 at D_2

We define that $P_{x_2}^{OP}$ as an event that transfers the best UAV or D_1 or D_2 can not successfully decode x_2 because the SINR/SNR is below threshold value γ_{th2}.

From (8), (11) and (12), the $P_{x_2}^{OP}$ is given by (see Eq. (28) in the next page).

$$P_{x_2}^{OP} = \Pr\left\{\gamma_{2,UAV_k} < \gamma_{th2} \text{ or } \gamma_{2,D2} < \gamma_{th2} \text{ or } \gamma_{2,D1} < \gamma_{th2}\right\}$$
$$= 1 - \Pr\left\{\frac{\Theta_2 P_{BS}|g_k|^2}{\Theta_1 P_{BS}|g_k|^2+1} > \gamma_{th2}, \frac{\Theta_2 P_{UAV}^X |h_2|^2}{\Theta_1 P_{UAV}^X |h_2|^2+1} > \gamma_{th2}, \frac{\Theta_2 P_{UAV}^X |h_1|^2}{\Theta_1 P_{UAV}^X |h_1|^2+1} > \gamma_{th2}\right\} \quad (28)$$

Eq. (28) can be rewritten by (see Eq. (29) in the next page)

$$P_{x_2}^{OP} = 1 - \Pr\left\{\begin{array}{l}\Theta_2 P_{BS}|g_k|^2 > \gamma_{th2}\left(\Theta_1 P_{BS}|g_k|^2 + 1\right), \frac{\Theta_2 \psi_E P_{BS}|g_k|^2|h_2|^2}{\Theta_1 \psi_E P_{BS}|g_k|^2|h_2|^2+1} > \gamma_{th2}, \\ \frac{\Theta_2 \psi_E P_{BS}|g_k|^2|h_1|^2}{\Theta_1 \psi_E P_{BS}|g_k|^2|h_1|^2+1} > \gamma_{th2}\end{array}\right\}$$
$$= 1 - \Pr\left\{A > \frac{\gamma_{th2}}{P_{BS}(\Theta_2 - \gamma_{th2}\Theta_1)}, AB > \frac{\gamma_{th2}}{P_{BS}\psi_E(\Theta_2 - \gamma_{th2}\Theta_1)}, AC > \frac{\gamma_{th2}}{P_{BS}\psi_E(\Theta_2 - \gamma_{th2}\Theta_1)}, \right\} \quad (29)$$

where $\psi_E = \beta\eta$ and $\psi_E = \frac{2\alpha\eta}{1-\alpha}$ represent EH for BS-based PSR and BS-based TSR protocols, respectively.

Proof see "Appendix 3".

It can be seen from (29) that the outage probability always satisfies $\gamma_{th2} > \frac{\Theta_2}{\Theta_1}$.

Therefore, we need to allocate more power for symbol x_1 to satisfy $\Theta_2 > \Theta_1\gamma_{th2}$. Thus, (29) can be expressed by (see Eq. (30) in the next page)

$$P_{x_2}^{OP} = 1 - \int_{t_1}^{\infty} \Pr\left\{B > \frac{t_1}{a}, C > \frac{t_1}{a}\right\} f_A(a)da = 1 - \int_{t_2}^{\infty}\int_{\frac{t_1}{a}}^{\infty} \Pr\left\{1 - F_B\left(\frac{t_1}{a}\right)\right\} f_C(c)f_A(a)dadc\,, \quad (30)$$

where $t_2 = \frac{\gamma_{th2}}{P_{BS}(\Theta_2 - \gamma_{th2}\Theta_1)}$ and $t_1 = \frac{\gamma_{th2}}{P_{BS}\psi_E(\Theta_2 - \gamma_{th2}\Theta_1)}$

From (30) and the transformations, the expression can be obtained by (see Eq. (31))

$$P_{x_2}^{OP} = 1 - \int_{t_2}^{\infty}\int_{\frac{t_1}{a}}^{\infty} \Pr\left\{1 - F_B\left(\frac{t_1}{a}\right)\right\} f_C(c)f_A(a)dadc$$
$$= 1 - \sum_{k=1}^{K} (-1)^{k-1}\binom{K}{k}\frac{k}{\Omega_2}\underbrace{\int_{t_2}^{\infty} \exp\left(-\frac{\tau}{a} - \frac{ka}{\Omega_2}\right)da}_{\chi}, \quad (31)$$

Proof see "Appendix 4".

where $\tau = \frac{t_1}{\Omega_3} + \frac{t_1}{\Omega_1}$. Since it is highly complex to calculate a closed-form expression, thus an approximate calculation method, namely Taylor series expansion, is utilized as the following expression

$$\exp\left(-\frac{u}{a}\right) = \sum_{n=0}^{K_t} \frac{(-1)^k}{k!}\left(\frac{u}{a}\right)^k, \quad (32)$$

where $K_t \in \{1, \ldots, \infty\}$.

Then, we obtain the following expression

$$\chi = \sum_{n=0}^{K_t} \frac{(-1)^k}{k!} \int_{t_2}^{\infty} \left(\frac{\tau}{a}\right)^k \exp\left(-\frac{ka}{\Omega_2}\right) da$$
$$= \sum_{n=0}^{K_t} \frac{(-1)^k \tau^n}{n!} \left(\frac{1}{t_2}\right)^{n-1} E_n\left(\frac{kt_2}{\Omega_2}\right), \tag{33}$$

where $E_n(.)$ is an exponential integral function.

Substituting (33) into (31), the $P_{x_2}^{OP}$ is given by (see Eq. (34) at the top of the next page)

$$P_{x_2}^{OP} = 1 - \sum_{k=0}^{K} \sum_{n=0}^{K_t} \frac{(-1)^k (-1)^n \beta^n}{n!} \binom{K}{k} \frac{k}{\Omega_2} \left(\frac{1}{t_2}\right)^{n-1} E_n\left(\frac{kt_2}{\Omega_2}\right) \tag{34}$$

4 Throughput

4.1 Throughput at UAV

The throughput at UAV_k is given by

$$\tau_{UAV_k} = \left(1 - P_{x_1}^{UAV_k}\right) R_{1,k} + \left(1 - P_{x_2}^{UAV_k}\right) R_{2,k}, \tag{35}$$

Where $P_{x_1}^{UAV_k}$ and $P_{x_2}^{UAV_k}$ are determined from (14) and (18), respectively. $R_{1,k}$ and $R_{2,k}$ are the rates to decode signal x_1 and x_2 at UAV_k, respectively.

4.2 Throughput at the User

For perfect SIC at the user, the throughput at user D_k is given by

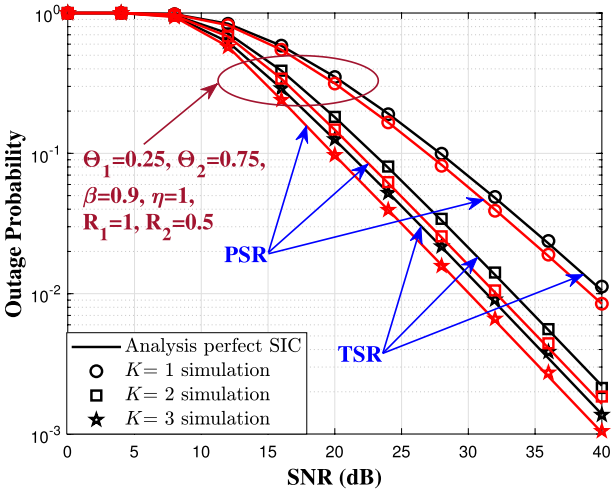

Fig. 4 The outage probability for decoding the signal x_1 with perfect SIC and varried UAV number

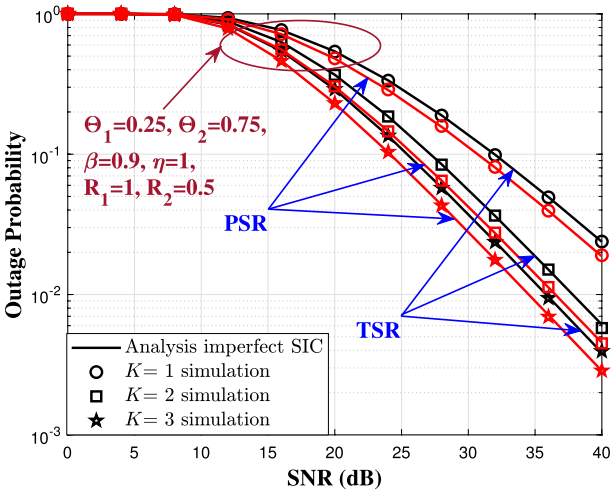

Fig. 5 The outage probability for decoding the signal x_1 with imperfect SIC and varried UAV number

$$\tau_{D_k}^{error} = \left(1 - P_{x_1}^{OP}\right) R_{1,k} + \left(1 - P_{x_2}^{OP}\right) R_{2,k} \tag{36}$$

For imperfect SIC at the user, the throughput at user D_k is given by

$$\tau_{D_k}^{ISIC} = \left(1 - P_{x_1,D_1}^{I\_SIC}\right) R_{1,k} + \left(1 - P_{x_2}^{OP}\right) R_{2,k} \tag{37}$$

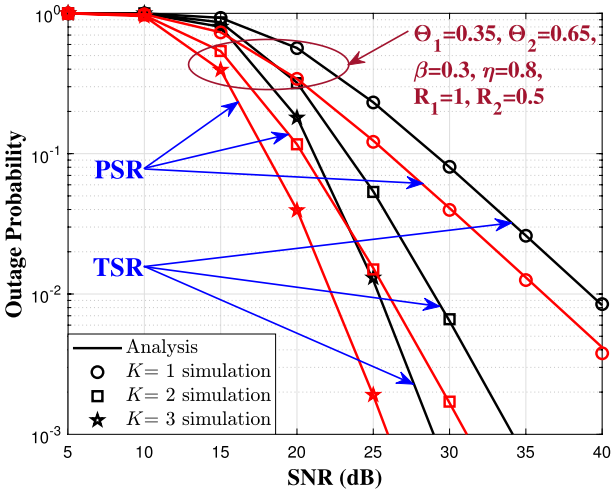

Fig. 6 The outage probability for decoding the signal x_2 at UAV$_k$ versus varried UAV number

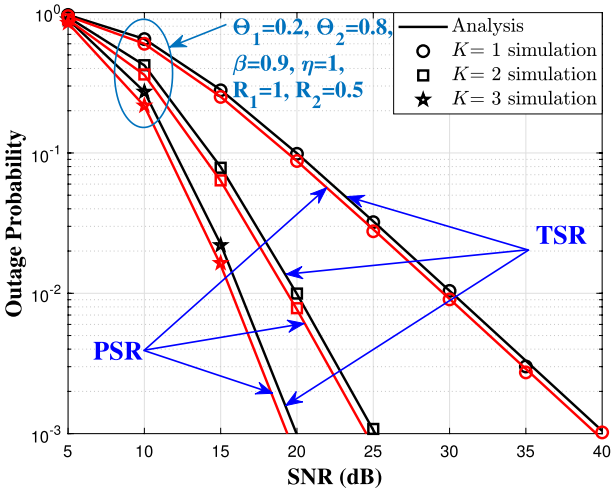

Fig. 7 The outage probability for decoding the signal x_2 at UAV$_k$ versus varried UAV number

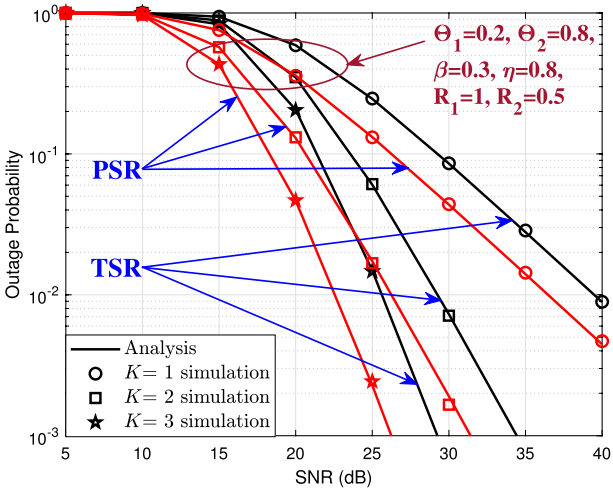

Fig. 8 The outage probability for decoding the signal x_1 at UAV$_k$ versus varried UAV number

5 Simulation Results

In this section, we provide several results to illustrate the effects of the number of relays, channel increasing level (distance or path-loss), and imperfect SIC for the RF energy harvesting efficiency of NOMA systems. The parameters of the system are set as follows. Because D_1 is closer to the relaying node than D_2, power allocation coefficients are $\Theta_1 = 0.2$ and $\Theta_2 = 0.8$ for D_1 and D_2, respectively. Bit rates are set $R_1 = 1$ (bpcu) and $R_2 = 0.5$ (bpcu) for D_1 and D_2, respectively.

The energy harvesting fraction in the BS-based TSR protocol is $\alpha = 0.3$. The channel gains are $\Omega_1 = \Omega_3 = 1$ and $\Omega_2 = 2$ and the energy conversion factor is $\eta = 1$.

Figures 4 and 5 show the comparison of the outage probability x_1 at D_1 and the average SNR in cases of perfect and imperfect SIC and varied UAV numbers. The power allocation coefficients for decoding x_1 and x_2 are $\Theta_1 = 0.25$, $\Theta_2 = 0.75$, respectively. It can be observed from these figures that the outage probability decreases significantly as the UAV

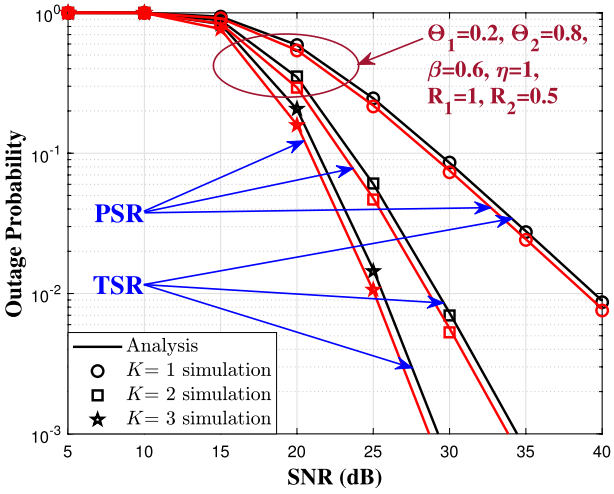

Fig. 9 The outage probability for decoding the signal x_1 at UAV$_k$ versus varried UAV number

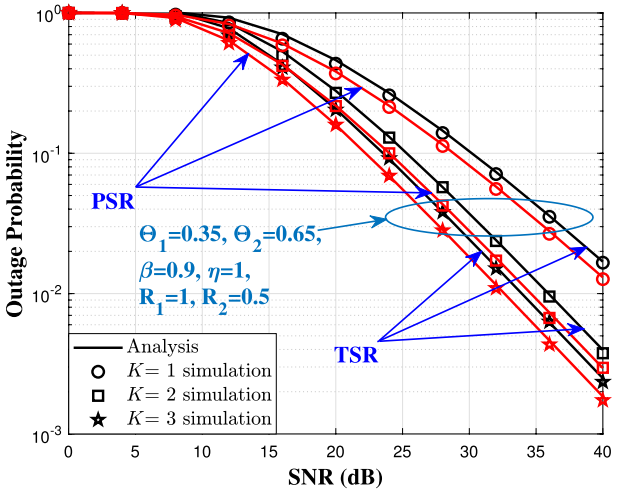

Fig. 10 The probability for decoding the signal x_2 at D_2 with the varied UAV number

number increases from 1 to 3 for perfect and imperfect SIC. Besides, the outage probability for perfect SIC is considerably lower than that for imperfect SIC. It proves that the efficiency of the system with perfect SIC is over the desired threshold level. In addition, the outage probability for BS-based PSR is also lower than that for BS-based TSR.

Figures 6, 7, 8, 9 describe the outage probabilities for decoding the signals x_2 and x_1 at the UAV, respectively. It is observed for both figures that the outage probability is low more and more as the number of UAVs increases from 1 to 3. It is proved that when the number of UAVs increases, the system is stable. Besides, the BS-based PSR has a lower outage probability than the BS-based TSR.

Figures 10 and 11 plot the outage probability for decoding x_2 at D_2 with the varied UAV number. In this figure, we use two PSR and TSR protocols corresponding with the varied UAV number. As shown in Figs. 10, 11, the outage probability is lower as the UAV number

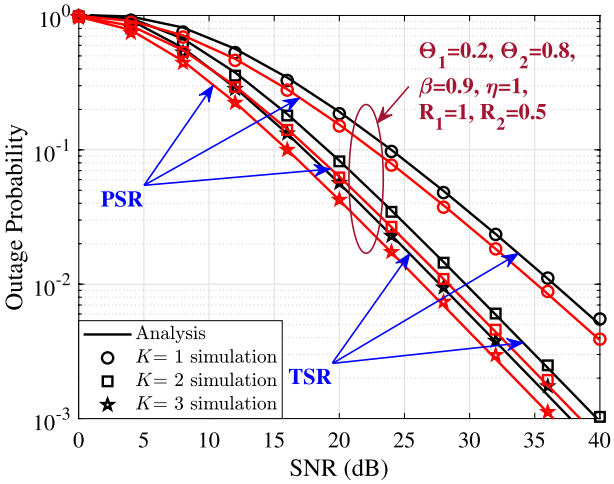

Fig. 11 The probability for decoding the signal x_2 at D_2 with the varied UAV number

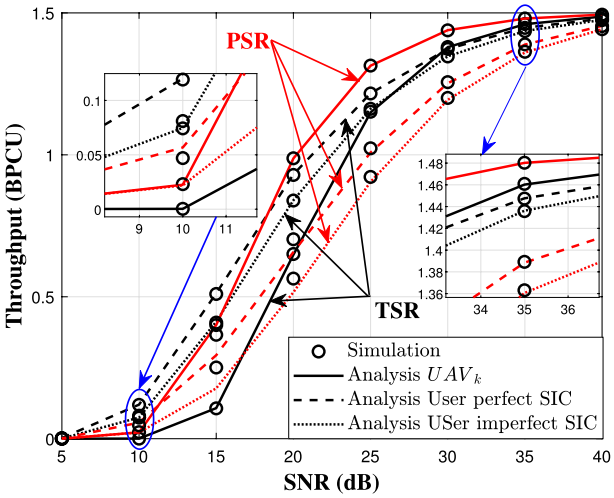

Fig. 12 The throughput of users in cases of perfect and imperfect SIC for BS-based PSR and BS-based TSR protocols

increases from 1 to 3. Furthermore, the outage probability for BS-based PSR is lower than that for BS-based TSR. The reason is that the best UAV is chosen to provide the best channel from the source to relay so that a better decoding efficiency and a higher energy harvesting efficiency from the source in the first phase can be achieved. We can see that the simulation results match the analytic results.

Figures 12 well as figure 13 plot the common throughput for two cases at UAV_k, and at two users D_1 and D_2. The BS-based PSR achieves the highest throughput at UAV_k as compared to the throughput at the users. The throughput threshold value is 1.5. The throughput at UAV_k for BS-based PSR protocol is higher than that for BS-based TSR. On the contrary, the throughput at the users for BS-based PSR is lower than that for BS-based TSR. Furthermore, from Fig. 13, we can also see that the throughput at the users in cases of perfect SIC is much better than the throughput at the users in cases of imperfect SIC.

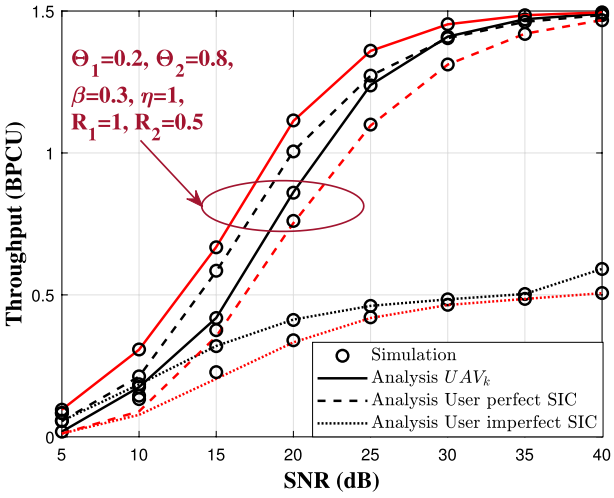

Fig. 13 The throughput of users in cases of perfect and imperfect SIC for BS-based PSR and BS-based TSR protocols

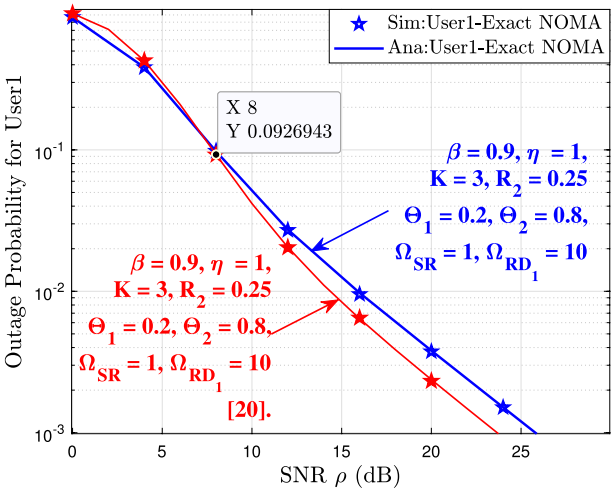

Fig. 14 Comparison of outage probability between this work and [20]

Figure 14 describes the comparison in terms of outage probability for User1-exact of NOMA scheme between our work and the work of [20]. The figure shows that the protocols for our work obtain a lower outage probability than that for the work of [20] in the SNR region of from 0 to 8 dB. In contrast, the protocols for our work obtain a slightly higher outage probability than that for the work of [20] in the SNR region of from 0 to 8 dB. It can be concluded that the higher the target rate, the higher the dropped data. This can be explained that the quality of propagation path of the NOMA downlink cooperative dual-hop relay system in [20] is better than our system model with UAVs in cooperative relaying networks in the SNR region of from 0 to 8 dB. In general, the work in [20] achieves slightly better performance than in our work when SNR increases (SNR > 8 dB).

6 Conclusion

Two BS-based PSR and BS-based TSR protocols for the NOMA system have been presented in this paper. The closed-form expressions of the outage probability and throughput for UAVs and users were derived. Particularly, the outage probabilities at cooperative relaying user's device, i.e., D_1, were also derived in closed-form expressions for perfect and imperfect SIC. The simulation results show that the outage probability and throughput for BS-based PSR protocol were superior to that for BS-based TSR protocol. The analytic results matched the simulation results. For future work, we can develop the system using multiple antennas at two users D_1 and D_2 to enhance the performance of the system.

Appendix 1

See Eq. (38), (39) are proof of Eq. (14). The proof is completed.

$$\begin{aligned}
P_{x_1}^{UAV_k} &= \Pr\left\{\gamma_{2,UAV_k} < \gamma_{th2}, \gamma_{1,UAV_k} < \gamma_{th1}\right\} \\
&= 1 - \Pr\left\{\frac{\psi_I\Theta_2 P_{BS}\left|g_k\right|^2}{\psi_I\Theta_1 P_{BS}\left|g_k\right|^2+1} > \gamma_{th1}, \psi_I\Theta_1 P_{BS}\left|g_k\right|^2 > \gamma_{th1}\right\} \\
&= 1 - \Pr\left\{\psi_I\Theta_2 P_{BS}A > \gamma_{th2}\left(\psi_I\Theta_1 P_{BS}A + 1\right), A > \frac{\gamma_{th1}}{\psi_I\Theta_1 P_{BS}}\right\} \\
&= 1 - \Pr\left\{\psi_I\Theta_2 P_{BS}A - \gamma_{th2}\psi_I\Theta_1 P_{BS}A > \gamma_{th2}, A > \frac{\gamma_{th1}}{\psi_I\Theta_1 P_{BS}}\right\} \\
&= 1 - \Pr\left\{A\psi_I P_{BS}\left(\Theta_2 - \gamma_{th2}\Theta_1\right) > \gamma_{th2}, A > \frac{\gamma_{th1}}{\Theta_1 P_{BS}}\right\} \\
&= 1 - \Pr\left\{A > \frac{\gamma_{th2}}{\psi_I P_{BS}\left(\Theta_2 - \gamma_{th2}\Theta_1\right)}, A > \frac{\gamma_{th1}}{\psi_I\Theta_1 P_{BS}}\right\} \\
&= \Pr\left\{A > \max\left(\frac{\gamma_{th2}}{\psi_I P_{BS}\left(\Theta_2 - \gamma_{th2}\Theta_1\right)}, \frac{\gamma_{th1}}{\psi_I\Theta_1 P_{BS}}\right)\right\}
\end{aligned} \tag{38}$$

Given $\varsigma = \max\left(\frac{\gamma_{th2}}{\psi_I P_{BS}\left(\Theta_2 - \gamma_{th2}\Theta_1\right)}, \frac{\gamma_{th1}}{\psi_I\Theta_1 P_{BS}}\right)$, $P_{x_1}^{UAV_k}$ can be rewritten by

$$\begin{aligned}
P_{x_1}^{UAV_k} &= 1 - \Pr\{A > \varsigma\} = 1 - F_A(\varsigma) \\
&= 1 - \sum_{k=1}^{K}(-1)^{k-1}\binom{K}{k}\exp\left(-\frac{k\varsigma}{\Omega_2}\right).
\end{aligned} \tag{39}$$

Appendix 2

See Eq. (40) is proof of Eq. (25). The proof is completed

$$
\begin{aligned}
P_{x_1,D_1}^{I\_SIC} &= \Pr\left[\min\left(\gamma_{1,UAV_k},\gamma_{1,D_1}\right) \le \gamma_{th1}\right] \\
&= 1 - \Pr\left[\min\left(\gamma_{1,UAV_k},\gamma_{1,D_1}\right) \ge \gamma_{th1}\right] \\
&= 1 - \Pr\left[\gamma_{1,UAV_k} \ge \gamma_{th1}, \gamma_{1,D_1} \ge \gamma_{th1}\right] \\
&= 1 - \Pr\left[\frac{\Theta_1 P_{BS}|g_k|^2}{\Theta_2\rho_2 P_{BS}|g_k|^2+1} \ge \gamma_{th1}, \frac{\Theta_1 P_{UAV}^X|h_1|^2}{\Theta_2\rho_1 P_{UAV}^X|h_1|^2+1} \ge \gamma_{th1}\right] \\
&= 1 - \Pr\left[\Theta_1 P_{BS}|g_k|^2 \ge \gamma_{th1}\left(\Theta_2\rho_2 P_{BS}|g_k|^2+1\right), \Theta_1 P_{UAV}^X|h_1|^2 \ge \gamma_{th1}\left(\Theta_2\rho_1 P_{UAV}^X|h_1|^2+1\right)\right] \\
&= 1 - \Pr\left[\Theta_1 P_{BS}|h_k|^2 \ge \gamma_{th1}\Theta_2\rho_2 P_{BS}|g_k|^2+\gamma_{th1}, \Theta_1 P_{UAV}^X|h_1|^2 \ge \gamma_{th1}\Theta_2\rho_1 P_{UAV}^X|h_1|^2+\gamma_{th1}\right] \\
&= 1 - \Pr\left[\Theta_1 P_{BS}|g_k|^2 - \gamma_{th1}\Theta_2\rho_2 P_{BS}|g_k|^2 \ge \gamma_{th1}, \Theta_1 P_{UAV}^X|h_1|^2 - \gamma_{th1}\Theta_2\rho_1 P_{UAV}^X|h_1|^2 \ge \gamma_{th1}\right] \\
&= 1 - \Pr\left[|g_k|^2 P_{BS}\left(\Theta_1 - \gamma_{th1}\Theta_2\rho_2\right) \ge \gamma_{th1}, |h_1|^2 P_{UAV}^X\left(\Theta_1 - \gamma_{th1}\Theta_2\rho_1\right) \ge \gamma_{th1}\right] \\
&= 1 - \Pr\left[|g_k|^2 \ge \frac{\gamma_{th1}}{P_{BS}\left(\Theta_1-\gamma_{th1}\Theta_2\rho_2\right)}, |h_1|^2 \ge \frac{\gamma_{th1}}{|g_k|^2\psi_E P_{BS}\left(\Theta_1-\gamma_{th1}\Theta_2\rho_1\right)}\right] \\
&= 1 - \Pr\left[A \ge \frac{\gamma_{th1}}{P_{BS}\left(\Theta_1-\gamma_{th1}\Theta_2\rho_2\right)}, C \ge \frac{\gamma_{th1}}{A\psi_E P_{BS}\left(\Theta_1-\gamma_{th1}\Theta_2\rho_1\right)}\right].
\end{aligned}
\tag{40}
$$

Appendix 3

See Eq. (41) is proof of Eq. (29). The proof is completed.

$$
\begin{aligned}
P_{x_2}^{OP} &= 1-\Pr\left\{\begin{array}{l}\Theta_2 P_{BS}|g_k|^2 > \gamma_{th2}\left(\Theta_1 P_{BS}|g_k|^2+1\right), \frac{\Theta_2\psi_E P_{BS}|g_k|^2|h_2|^2}{\Theta_1\psi_E P_{BS}|g_k|^2|h_2|^2+1} > \gamma_{th2},\\ \frac{\Theta_2\psi_E P_{BS}|g_k|^2|h_1|^2}{\Theta_1\psi_E P_{BS}|g_k|^2|h_1|^2+1} > \gamma_{th2}\end{array}\right\}\\
&= 1-\Pr\left\{\begin{array}{l}\Theta_2 P_{BS}|g_k|^2 > \gamma_{th2}\left(\Theta_1 P_{BS}|g_k|^2+1\right),\\ \Theta_2\psi_E P_{BS}|g_k|^2|h_2|^2 > \gamma_{th2}\left(\Theta_1\psi_E P_{BS}|g_k|^2|h_2|^2+1\right),\\ \Theta_2\psi_E P_{BS}|g_k|^2|h_1|^2 > \gamma_{th2}\left(\Theta_1\psi_E P_{BS}|g_k|^2|h_1|^2+1\right)\end{array}\right\}\\
&= 1-\Pr\left\{\begin{array}{l}\Theta_2 P_{BS}|g_k|^2 > \gamma_{th2}\Theta_1 P_{BS}|g_k|^2+\gamma_{th2},\\ \Theta_2\psi_E P_{BS}|g_k|^2|h_2|^2 > \gamma_{th2}\Theta_1\psi_E P_{BS}|g_k|^2|h_2|^2+\gamma_{th2},\\ \Theta_2\psi_E P_{BS}|g_k|^2|h_1|^2 > \gamma_{th2}\Theta_1\psi_E P_{BS}|g_k|^2|h_1|^2+\gamma_{th2}\end{array}\right\}\\
&= 1-\Pr\left\{\begin{array}{l}\Theta_2 P_{BS}|g_k|^2-\gamma_{th2}\Theta_1 P_{BS}|g_k|^2 > \gamma_{th2},\\ \Theta_2\psi_E P_{BS}|g_k|^2|h_2|^2-\gamma_{th2}\Theta_1\psi_E P_{BS}|g_k|^2|h_2|^2 > \gamma_{th2},\\ \Theta_2\psi_E P_{BS}|g_k|^2|h_1|^2-\gamma_{th2}\Theta_1\psi_E P_{BS}|h_k|^2|h_1|^2 > \gamma_{th2}\end{array}\right\}\\
&= 1-\Pr\left\{\begin{array}{l}|g_k|^2 P_{BS}\left(\Theta_2-\gamma_{th2}\Theta_1\right) > \gamma_{th2}, |g_k|^2|h_2|^2 P_{BS}\psi_E\left(\Theta_2-\gamma_{th2}\Theta_1\right) > \gamma_{th2},\\ |g_k|^2|h_1|^2 P_{BS}\psi_E\left(\Theta_2-\gamma_{th2}\Theta_1\right) > \gamma_{th2}\end{array}\right\}\\
&= 1-\Pr\left\{\begin{array}{l}|g_k|^2 > \frac{\gamma_{th2}}{P_{BS}\left(\Theta_2-\gamma_{th2}\Theta_1\right)}, |g_k|^2|h_2|^2 > \frac{\gamma_{th2}}{P_{BS}\psi_E\left(\Theta_2-\gamma_{th2}\Theta_1\right)},\\ |g_k|^2|h_1|^2 > \frac{\gamma_{th2}}{P_{BS}\psi_E\left(\Theta_2-\gamma_{th2}\Theta_1\right)}\end{array}\right\}\\
&= 1-\Pr\left\{\begin{array}{l}A > \frac{\gamma_{th2}}{P_{BS}\left(\Theta_2-\gamma_{th2}\Theta_1\right)}, AB > \frac{\gamma_{th2}}{P_{BS}\psi_E\left(\Theta_2-\gamma_{th2}\Theta_1\right)},\\ AC > \frac{\gamma_{th2}}{P_{BS}\psi_E\left(\Theta_2-\gamma_{th2}\Theta_1\right)}\end{array}\right\}.
\end{aligned}
\tag{41}
$$

Appendix 4

Similarly, Eq. (42) is proof of Eq. (31). The proof is completed.

$$
\begin{aligned}
P_{x_2}^{OP} &= 1 - \int_{t_2}^{\infty} \int_{\frac{t_1}{a}}^{\infty} \Pr\left\{1 - F_B\left(\frac{t_1}{a}\right)\right\} f_C(c) f_A(a) da dc \\
&= 1 - \int_{t_2}^{\infty} \int_{\frac{t_1}{a}}^{\infty} \left\{1 - \left(1 - \exp\left(-\frac{t_1}{\Omega_1 a}\right)\right)\right\} \frac{1}{\Omega_3} \exp\left(-\frac{z}{\Omega_3}\right) \sum_{k=1}^{K} (-1)^{k-1} \binom{K}{k} \frac{k}{\Omega_2} \exp\left(-\frac{ka}{\Omega_2}\right) dc da \\
&= 1 - \sum_{k=1}^{K} (-1)^{k-1} \binom{K}{k} \frac{k}{\Omega_2} \int_{t_1}^{\infty} \int_{\frac{t_1}{a}}^{\infty} \exp\left(-\frac{t_1}{\Omega_1 a}\right) \frac{1}{\Omega_3} \exp\left(-\frac{c}{\Omega_3}\right) \exp\left(-\frac{ka}{\Omega_2}\right) dc da \\
&= 1 - \sum_{k=1}^{K} (-1)^{k-1} \binom{K}{k} \frac{k}{\Omega_2} \int_{t_2}^{\infty} \int_{\frac{t_1}{a}}^{\infty} \frac{1}{\Omega_3} \exp\left(-\frac{c}{\Omega_3}\right) dc \exp\left(-\frac{t_1}{\Omega_1 a}\right) \exp\left(-\frac{ka}{\Omega_2}\right) da \\
&= 1 - \sum_{k=1}^{K} (-1)^{k-1} \binom{K}{k} \frac{k}{\Omega_2} \int_{t_2}^{\infty} \left(\frac{1}{-\frac{1}{\Omega_3}} \exp\left(-\frac{z}{\Omega_3}\right) \Big|_{\frac{t_1}{x}}^{\infty} \right) \exp\left(-\frac{t_1}{\Omega_1 a}\right) \exp\left(-\frac{ka}{\Omega_2}\right) da \\
&= 1 - \sum_{k=1}^{K} (-1)^{k-1} \binom{K}{k} \frac{k}{\Omega_2} \int_{t_2}^{\infty} \left(-\left(\exp(-\infty) - \exp\left(-\frac{\frac{t_1}{a}}{\Omega_3}\right)\right)\right) \exp\left(-\frac{t_1}{\Omega_1 a}\right) \exp\left(-\frac{ka}{\Omega_2}\right) da \\
&= 1 - \sum_{k=1}^{K} (-1)^{k-1} \binom{K}{k} \frac{k}{\Omega_2} \int_{t_2}^{\infty} \left(-\left(0 - \exp\left(-\frac{t_1}{a\Omega_3}\right)\right)\right) \exp\left(-\frac{t_1}{\Omega_1 a}\right) \exp\left(-\frac{ka}{\Omega_2}\right) da \\
&= 1 - \sum_{k=1}^{K} (-1)^{k-1} \binom{K}{k} \frac{k}{\Omega_2} \int_{t_1}^{\infty} \exp\left(-\frac{t_1}{\Omega_3 a}\right) \exp\left(-\frac{t_1}{\Omega_1 a}\right) \exp\left(-\frac{ka}{\Omega_2}\right) da \\
&= 1 - \sum_{k=1}^{K} (-1)^{k-1} \binom{K}{k} \frac{k}{\Omega_2} \int_{t_2}^{\infty} \exp\left(-\frac{t_1}{\Omega_3 a} - \frac{t_1}{\Omega_1 a} - \frac{ka}{\Omega_2}\right) da \\
&= 1 - \sum_{k=1}^{K} (-1)^{k-1} \binom{K}{k} \frac{k}{\Omega_2} \int_{t_2}^{\infty} \exp\left(-\left(\frac{t_1}{\Omega_3} + \frac{t_1}{\Omega_1}\right)\frac{1}{a} - \frac{ka}{\Omega_2}\right) da \\
&= 1 - \sum_{k=1}^{K} (-1)^{k-1} \binom{K}{k} \underbrace{\frac{k}{\Omega_2} \int_{t_2}^{\infty} \exp\left(-\frac{\tau}{a} - \frac{ka}{\Omega_2}\right) da}_{\chi}.
\end{aligned}
\tag{42}
$$

Acknowledgements The author would like to thank the anonymous Reviewers for his/her efforts in spending time to process the author's paper.

Author Contributions HQT: conceptualization, methodology, software, formal analysis, investigation; HQT: data curation, writing-original draft preparation; HQT: validation, resources; HQT: writing-reviewing and editing.

Declarations

Conflict of interest The author declares there is no conflict of interest in this manuscript.

References

1. Zeng, Y., Lyu, J., & Zhang, R. (2018). Cellular-connected UAV: Potential, challenges, and promising technologies. *IEEE Wireless Communications, 26*(1), 120–127.
2. Luo, X., Zhang, Y,, He, Z., & Yang, G.. (2019). Zijie Ji. IEEE Access: A Two-Step Environment-Learning-Based Method for Optimal UAV Deployment.
3. Zhao, N., Lu, W., Sheng, M., Chen, Y., Tang, J., Yu, F. R., & Wong, K. K. (2019). UAV-assisted emergency networks in disasters. *IEEE Wireless Communications, 26*(1), 45–51.
4. Liu, Y., Qin, Z., Cai, Y., Gao, Y., Li, G. Y., & Nallanathan, A. (2019). UAV communications based on non-orthogonal multiple access. *IEEE Wireless Communications, 26*(1), 52–57.
5. Baghani, M., Parsaeefard, S., Derakhshani, M. & Saad, W. (2019). Dynamic non-orthogonal multiple access (NOMA) and orthogonal multiple access (OMA) in 5G wireless networks. *IEEE Transactions on Communications*, 1,
6. Islam, S. R., Avazov, N., Dobre, O. A., & Kwak, K. S. (2016). Power-domain non-orthogonal multiple access (NOMA) in 5G systems: Potentials and challenges. *IEEE Communications Surveys Tutorials, 2*, 721–742.
7. Tran, H. Q., Nguyen, T. T., Phan, C. V. & Vien, Q. T. (2019). A power-splitting relaying protocol for wireless energy harvesting and information processing in NOMA systems. *IET Communications*, 2132–2140.
8. Tran, H. Q., Phan, C. V., & Vien, Q. T. (2020). Power splitting versus time switching based cooperative relaying protocols for SWIPT in NOMA systems. *Physical Communication, 41,* 101098.
9. Liu, G., Wang, Z., Hu, J., Ding, Z. & Fan, P. (2019). Cooperative NOMA broadcasting/multicasting for low-latency and high-reliability 5G cellular V2X communications. *IEEE Internet of Things Journal*.
10. Vaezi, M., Ding, Z., & Poor, H. V. (eds). (2019). Multiple access techniques for 5G wireless networks and beyond. *Springer*.
11. Zhou, F., Wu, Y., Hu, R. Q., Wang, Y., & Wong, K. K. (2018). Energy-efficient NOMA enabled heterogeneous cloud radio access networks. *IEEE Network, 2*, 152–160.
12. Tran, H. Q., Phan, C. V., & Vien, Q. T. (2021). Performance analysis of power-splitting relaying protocol in SWIPT based cooperative NOMA systems. *EURASIP Journal on Wireless Communications and Networking*, 110.
13. Mei, W., & Zhang, R. (2019). Uplink cooperative NOMA for cellular-connected UAV. *IEEE Journal of Selected Topics in Signal Processing, 13*(3), 644–656.
14. Sharma, P. K., & Kim, D. I., (2017). UAV-enabled downlink wireless system with non-orthogonal multiple access. *IEEE Globecom Workshops (GC Wkshps)*, 1–6.
15. Lyu, J., Zeng, Y., & Zhang, R. (2016). Cyclical multiple access in UAV-aided communications: A throughput-delay tradeoff. *IEEE Wireless Communications Letters, 5*(6), 600–603.
16. Zhao, N., Pang, X., Li, Z., Chen, Y., Li, F., Ding, Z., & Alouini, M. S. (2019). Joint trajectory and precoding optimization for UAV-assisted NOMA networks. *IEEE Transactions on Communications, 67*(5), 3723–3735.
17. Sohail, M. F., Leow, C. Y., & Won, S. (2018). Non-orthogonal multiple access for unmanned aerial vehicle assisted communication. *IEEE Access, 6*, 22716–22727.
18. Xu, J., Zeng, Y., & Zhang, R. (2018). UAV-enabled wireless power transfer: Trajectory design and energy optimization. *IEEE Transactions on Wireless Communications, 17*(8), 5092–5106.

19. Yin, S., Tan, J., & Li, L. (2017). UAV-assisted cooperative communications with wireless information and power transfer. arXiv preprint arXiv:1710.00174.
20. Lee, S., Da Costa, D. B., Vien, Q. T., Duong, T. Q., & de Sousa, R. T. (2017). Non-orthogonal multiple access schemes with partial relay selection. *IET Communications, 11*(6), 846–854.

Huu Q. Tran received the M.S degree in ElectronicsEngineering from Ho Chi Minh City University of Technologyand Education (HCMUTE), Viet Nam, in 2010. Currently, he hasbeen working as a lecturer at Faculty of Electronics Technology,Industrial University of Ho Chi Minh City (IUH), Viet Nam. Heis also a PhD candidate at Faculty of Electrical - ElectronicsEngineering, Ho Chi Minh City University of Technology andEducation, Viet Nam. His research interests include Wireless Communications, NonorthogonalMultiple Access (NOMA), Energy Harvesting (EH), Wireless CooperativeRelaying Networks, Heterogeneous Networks (HetNet), Cloud Radio Access Networks(C-RAN), Unmanned Aerial Vehicles (UAV), and Internet of Things (IoT).